



MICROSTRUCTURAL CHARACTERISTICS OF DISPERSION STRENGTHENED Cu-BASED SYSTEM

O. VELGOSOVÁ¹, I. SAXL² AND M. BESTERCI¹

¹*Institute of Materials Research SAS, Watsonova 47,
043 53 Košice Slovak Republic*

²*Mathematical Institute of Academy of Science of Czech Republic, Žitná 25,
11 67 Praha 1, Czech Republic*

ABSTRACT

The estimation of matrix grain size and volume fraction of dispersed phase in a real material is presented. Experimental material was prepared by powder metallurgy method of mechanical alloying. Microstructural data were obtained by the inference from planar sections.

The aim of work was the structural description of Cu 0.1% Al₂O₃ material by means of inference from planar section. Grain size estimation was carried out by combining the both line intercept and planar profile counts. The results were compared with the procedures recommended by the ASTM E-112 Standards.

KEYWORDS

Grain size, dispersed phase, profile and intercept counts.

INTRODUCTION

The uniform equiaxed grain structure of the examined system is suitable for a detailed metallographic analysis based on the grain size estimation methods recommended by the National Standards [1] and closely imitating the approaches proposed by ASTM E-112 Standards [2]. In particular, it supply a possibility to compare the assumptions inherent to Standards with the recent results obtained by stochastic simulations of space-filling cell systems - random Voronoi tessellations - in the case of one real grain structure [3].

MATERIALS AND MEASUREMENT

The material with the nominal volume fraction 1 vol.% Al₂O₃ was prepared by the method of reaction milling [4, 5]. The fundamental operation was homogenization milling of powder alloy CuAl with Al powder in oxidation atmosphere in an attritor, which resulted in the formation of CuO. During the subsequent heat treatment, oxygen passed from CuO to Al thus giving rise to the Al₂O₃ phase. The excess of CuO was removed by annealing in H₂+H₂O

atmosphere. The mixture was compacted by cold pressing, sintering and hot extrusion at temperature 750 - 800°C.

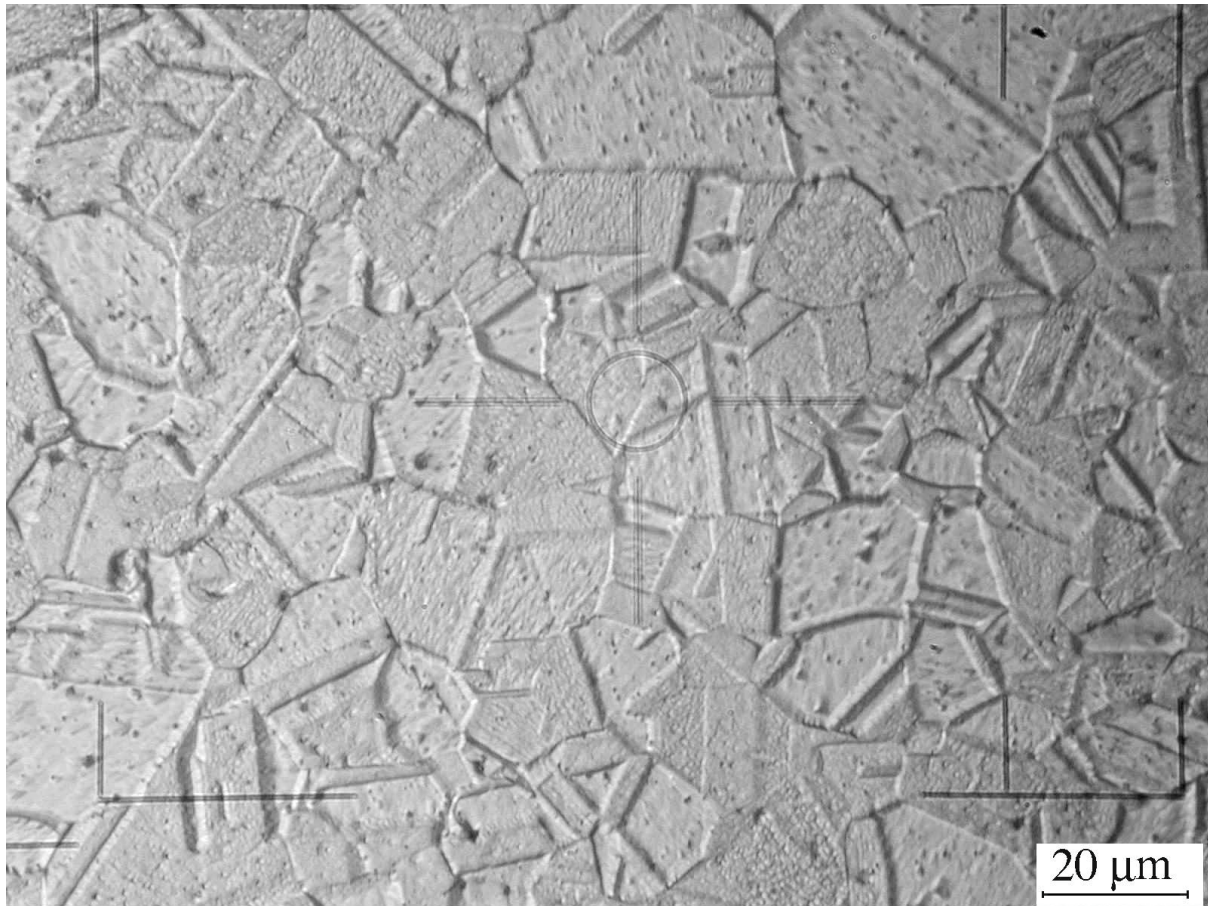


Fig. 1 Example of original analysed section.

Five similar metallographic specimens were prepared by polishing and etching in the water solution of the ammonium peroxodisulfate $(\text{NH}_4)_2\text{S}_2\text{O}_8$ and then observed in the light microscope under the magnification 1000 \times .

The manual analysis was performed on the microphotographs obtained by digital processing under the final magnification 1530 \times . The results obtained from five microphotographs of the area of 503 cm^2 containing in the average approximately 25 grain profiles were evaluated. The total number $N = 122$ profiles is well above the lower bound of 50 profiles recommended by the Standards. The observed grain profiles were equiaxial, heavily twinned and of a uniform size - Fig. 1. After a careful inspection, grain profiles could have been reliably and unequivocally identified in spite of somewhat confusing effect of twins - Fig. 2.

ESTIMATION METHODS

The volume fraction V_V of the dispersed Al_2O_3 particles was estimated by the lattice point count.

The both Jeffries and Heyn methods, namely profile and intercept counts, have been applied in order to obtain simultaneously the estimates of the profile intensity (density) N_A and of the intercept intensity (density) N_L : $[N_A] = (p_1 + 0.5 p_2 - 1)/W$, where p_1, p_2 are the numbers of profiles completely included within and cutting the measuring window of area W , resp., $[N_L] = (c_1 + 0.5 c_2)/L$, where c_1, c_2 are the numbers of chords completely and partly included within a test line of length L , respectively. Simultaneously, the chords lengths l have been directly measured: their mean length is $[E]l = 1/[N_L]$, CV l is their coefficient of variation.

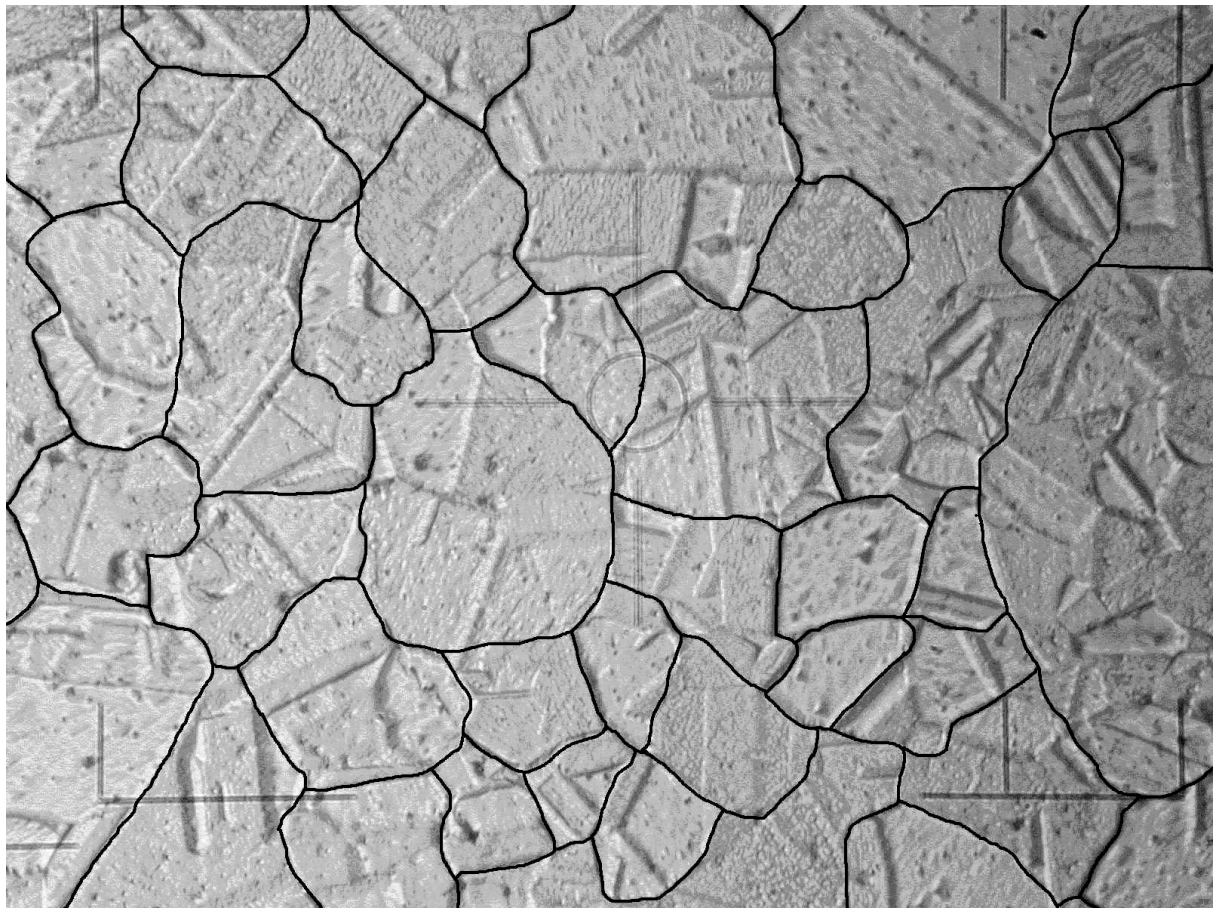


Fig. 2 The same section as in Fig. 1 with drawn up grain boundary traces.

The estimator of the mean profile area is $[Ea] = 1/[N_A]$. Areas of profiles completely included within measuring window were estimated by the lattice point count (lattice constant 1 cm). The coefficient of variation of such a size-weighted sample (the window boundary samples the profiles by their mean breadths) was used as a rough estimate of the coefficient of variation CV a of the whole induced planar tessellation.

The assumptions included in the Standards are as follows:

- I. There is a fixed relation between N_L and N_A , namely $N_A = cN_L^2$, where $c = 1/1.26 = 0.7937$. (The underlying idea is that the actual system of profile random chords is equivalent to the system of uniform random chords of one circle of area $1/N_A$ and a small correction is made thereafter).

Corollary: The estimates of the grain size number G based on N_L and N_A are identical, namely

$$G = -3.2877 + 6.6439 \log N_L = -2.9542 + 3.3220 \log N_A. \quad (1)$$

II. There is a fixed relation between the spatial grain intensity N_V and the planar feature intensities N_L, N_A (the underlying idea is that the system of profile chords is equivalent to the system of uniform random chords of a ball the volume of which is $1/N_V$).

Corollary: The estimates of the spatial grain intensity N_V based on N_L and N_A are identical, namely

$$N_V = c'' N_L^3 = c' N_A^{3/2}, \text{ where } c'' = 0.5659, c' = 0.81 \quad (2)$$

and further $c = (c''/c')^{2/3}$ as a consequence of the assumption I.

Table 1. Coefficients of variation and scale independent factors in different tessellations

Type of tessellation	CV l	CV a	CV v	c	c'	c''
Tetraikadekahedron (bc lattice)	0.471	0.532	0	0.756	0.648	0.426
rhomb. Dodekahedron (fc lattice)	0.476	0.565	0	0.770	0.620	0.419
Poisson -Voronoi tessellation	0.582	0.695	0.423	0.688	0.568	0.324
Johnson-Mehl model [6]	0.68	1.05	1.5	0.777	0.827	0.566
Poisson globular tessell. $N = 30$	0.75	1.14	1.67	0.71	0.84	0.50

A natural question whether there exists some spatial tessellation for which such assumptions are valid with a reasonable accuracy has been answered by Horálek [6]: it is the non-homogeneous Johnson-Mehl model with the rate of germ nucleation $I = \alpha t$, where t is time and α is an arbitrary constant. The stochastic simulations carried out by Saxl and Ponížil [3] have shown that there are also several convex tessellations for which the ASTM assumptions are approximately valid. However, all such tessellations are far from being reasonably uniform as may be seen from the values of their coefficients of variation. Several tessellations are compared in Tab.1. In the first two rows are isohedral tilings (Voronoi cells generated by body centered (bc) and face centered (fc) cubic translation lattices); the tetraikadekahedronal tessellation has the lowest possible values of CV a and CV l . In the last row is the tessellation generated by the Neyman-Scott cluster field with clusters of N Poisson distributed points embedded uniformly at random in a very small ball (for details see [3, 7]) with a moderately high value of CV a describing a bimodal tessellations with a great distance between the modes of the cell volume distribution.

RESULTS AND DISCUSSION

i) Volume fraction of Al_2O_3

The spatial distribution of the Al_2O_3 precipitates was rather non-uniform as shows the range of V_V in the five analysed samples -Tab. 2. The expected volume fraction V_V is higher; perhaps the size of some particles lies below resolution power of the microphotograph - their mean width was typically between 1 and 3 μm .

Table 2. Volume fraction estimation (lattice point count)

Volume fraction V_V [vol.%]	Range of V_V [vol.%]	Coefficient of error CE V_V	CV V_V
0.604	0.48 - 0.83	0.08	0.98

ii) *Estimation of the size of planar features*

Grain size estimation was realised by the linear method - Tab. 3. - and by planar method - Tab. 4. The value in parentheses of $[E/l]$ corresponds to equivalent convex profiles (see below). The grain size numbers G were calculated according to the two - by ASTM Standards equivalent - equation (1). The results differ only by 5% thus confirming that the assumption I is reasonably acceptable for the examined material. This conclusion has relatively general validity as it is shown in a more detailed study [7].

Table 3. Intercepts count (Heyn method) and chord length estimation

Number of chords	Mean chord length $[E/l] = [1/N_L]$ [mm]	Coefficient of error CE l	$[CV l]$	$[G]$
385	0.022 (0.024)	0.027	0.55	7.72 (7.47)

Table 4. Profiles count (Jeffries method) and profile area estimation

Number of profiles	Examined area [mm ²]	Mean profile area $[Ea] = [1/N_A]$ [mm ²]	Coefficient of error CE a	$[CV a]$	$[G]$
122	0.0215	7.7×10^{-4}	0.04	0.57	7.39

Table 5 summarises the values of the all scale invariant factors c , c' , c'' postulated in Standards [1, 2] and gives also the mean value of $[c] = N_A/N_L^2$ estimated separately for each of five examined specimens together with the corresponding standard deviation of the mean. The value is substantially lower than that one postulated by the ASTM Standards.

Table 5. Scale invariant factors

Source	c'	c''	c
ASTM	0.8	0.566	0.794
SK, CZ	1.0	0.7	0.788
Estimated	0.56 (0.60)	0.293 (0.398)	0.65±0.03 (0.76±0.03)

iii) *Estimation of the spatial grain size*

The estimates of the spatial grain intensity N_V calculated according to the recommendations of the Standards [2] are presented in Tab. 6; the value based on the intercept intensity N_L is by 60% higher than the estimate based on the profile intensity N_A .

Table 6. Estimates of the spatial grain intensity N_V

Specimens	$[N_V] = c' N_A^{1.5}$	$[N_V] = c'' N_L^3$
ASTM	37 411	53 140
Est. by w-s diagram	26 210 (28 080)	26 210 (28 080)

Using the estimates of CV a and c for the examined materials (Tables 4, 5), more realistic estimates of the factors c' , c'' valid for the examined material can be obtained using the recently proposed tool of analysis called the $w - s$ diagram [3]. In this diagram the relevant part of which is depicted in Fig. 3, every unit tessellation is represented by a point in the

orthogonal coordinate system with axes E_w (the mean value of the cell mean breadth w , called also the mean Feret diameter) and E_s (the mean cell surface). The upper and right non-linear scales show the values of the factors c' , c'' , which are, in general, the following functions of coordinates: $c' = (E_w)^{-3/2}$, $c'' = (4/E_s)^{-3}$ [3]. The net of dashed curves shows the relation between E_w and E_s at a constant value of the factor c , namely $E_s = 4(E_w/c)^{1/2}$ for selected values of c (2/3, 0.79 - ASTM value, 1). Other curves describe important tessellations dependent on some parameter. The thick dash-dotted curve (JM) describes the already mentioned Johnson-Mehl tessellation [6] with a variable rate of the nucleation intensity $I(t) = \alpha t^{\beta-1}$, the special case $\beta = 2$ of which approximately corresponds to the ASTM choice of factors c' , c'' - the ASTM point is denoted by the black circle lying slightly below the curve. The starting point ($\beta = 0$) of the JM curve is the Poisson-Voronoi tessellation (PVT). Diamond symbols denote the positions of tetrakaidecahedral (bc) and rhombic dodecahedral (fc) tilings and the curves joining these points with the PVT point represent so called displaced lattice tessellations generated by the corresponding lattices with randomly shifted lattice points. The shift distribution is the normal $N(0, u^2)$ with $0 \leq u \leq 10$; the tessellations differ only negligibly from PVT at the upper bound of u .

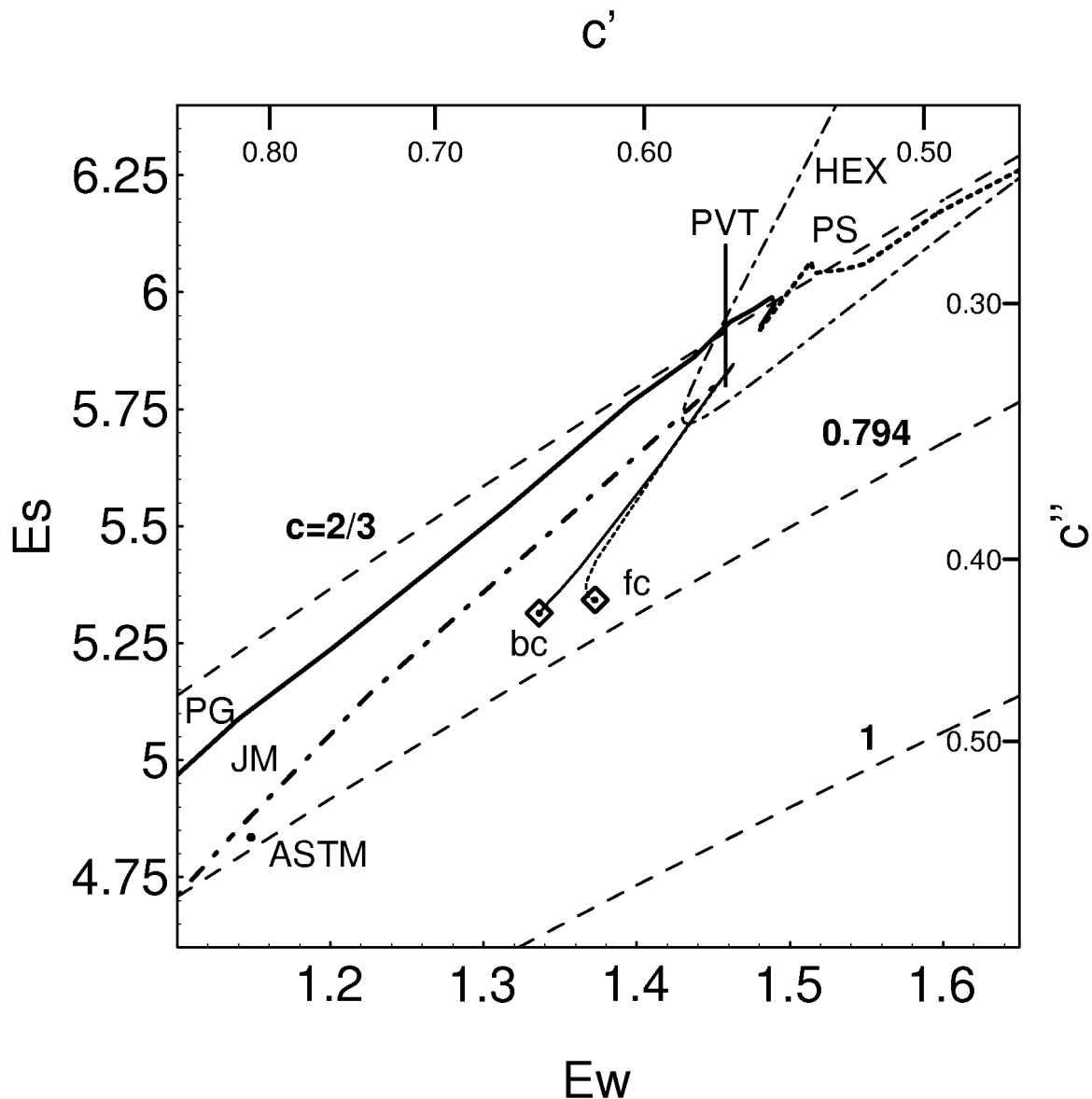


Fig. 3 Part of the w - s diagram (see the description in the text).

The thin dash-dotted curve (HEX) in the right upper corner of the diagram describes tilings by hexagonal prisms with a variable c/a ratio: on the left branch lie rods, on the right one lie plates. Finally, thick diagonal curve describes tessellations generated by Neyman-Scott cluster fields. Clusters are either of the globular type (PG - full line) described above or of the similar spherical type with points scattered uniformly at random on the sphere (PS - dotted line).

The part of the diagram below its diagonal belongs to mixtures of flat, rod-like and wedge-like cells with high size dispersion, whereas between PG and JM curves are concentrated tessellations of equiaxial highly dispersed cells [3]. The area above the diagonal is perhaps filled up by tessellations with non-convex corrugated fractal-like cell boundaries (high values of E_s at a given value of E_w).

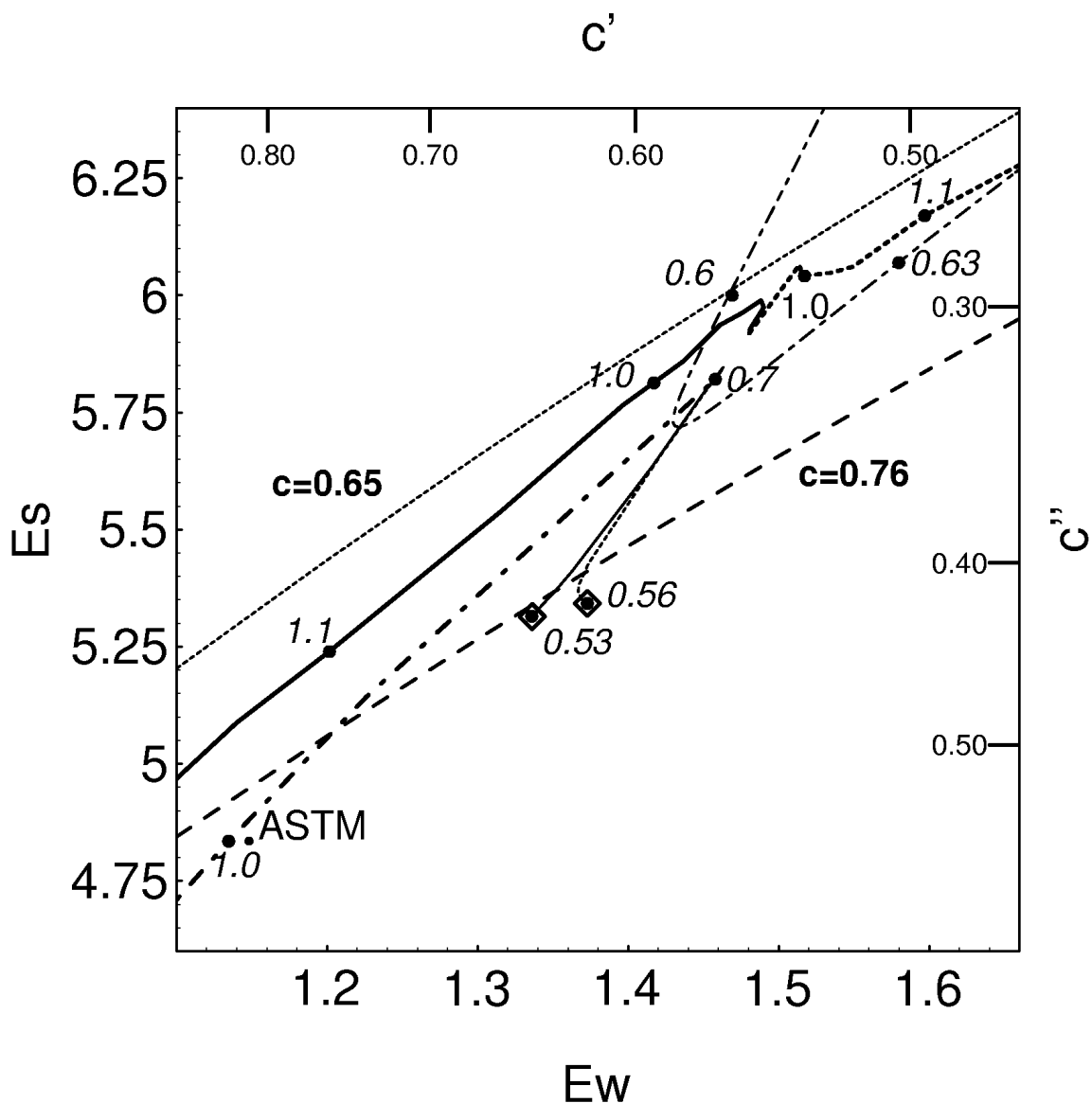


Fig. 4 $w - s$ diagram with the values of $CV a$ in selected points (see the description in the text).

In Fig. 4, the same curves are plotted with the values of $CV a$ in selected points. The minimum value of $CV a$ is at the bc point. According to our present knowledge, $CV a$

increases when moving from this point to the right upper and left lower corners (*i.e.* along the diagonal direction) and also when moving in the horizontal direction to the right side of the diagram (see [8]). Instead of the dashed net $c = \text{const.}$ in the Fig. 3, the dotted curve $c = 0.65$ is plotted corresponding to the estimated value of the c factor (Tab. 5). This value is somewhat low and the estimated value of $CV a = 0.57 \pm 0.01$ locates its probable position at the curve describing tilings by hexagonal rods in the point with $Ew = 1.47$ from which follow the estimates of the scale independent factors c' , c'' given in the last row of Tab. 5. However, the images of sections do not resemble sections of tiling by rods and a much more probable explanation of the low c value is the plain non-convexity of grains which decreases the value of Es and hence also of c . Consequently, the comparison with convex tessellations in the w - s diagram is not completely correct. In order to test this hypothesis, profiles have been made convex by replacing wavy grain boundary traces by straight segments joining the triple points. This procedure does not change the value of N_A but increases El by 9% and c by 18% - see the values in parentheses in the Tables 3 and 5. By inspection of the w - s diagram along the dashed curve $c = 0.76$, the position $Ew = 1.4$ can be tentatively assigned to the examined structure. The estimates of c' , c'' are again shown in Tab. 5 (the values in parentheses).

The improved estimates of the spatial grain intensity are presented in Tab. 6. They are considerably smaller than the estimates obtained by the ASTM approach which is not surprising as it tacitly assumes a value $CV a \approx 1$ describing a greater grain size dispersion than that one observed in the examined material. Moreover, there is no difference between the estimates based on either line intercept or profile intensities as the correct value of c is used to calculate c'' from estimated c' .

Finally, the empirical relations proposed in [3, 8] can be used to estimate the coefficient of variation $CV v$ from the values of $CV a$, $CV l$ (the relations hold for $0.53 < CV a < 0.9$, $0.47 < CV l < 0.7$):

$$[CV v]_{CV l} = 1.674 + 2.25 \ln(CV l) = 0.33,$$

$$[CV v]_{CV a} = 0.984 + 1.445 \ln(CV a) = 0.14.$$

The lower value of $[CV v]_{CV a}$ is not surprising as $CV a$ was necessarily underestimated by taking for its estimate the coefficient of variation of the sample containing only profiles completely included in the observing window. However, the both estimates clearly manifest that the grain volume has a very low dispersion.

CONCLUSIONS

- 1) Estimated volume fraction of Al_2O_3 secondary phase (0.604 vol.%) is essentially lower than the nominal volume fraction (1 vol.%). The plausible explanation is that only a fraction of greater particles was properly recognized on the microphotographs.
- 2) The profile size estimation by the both profile and intercept counts led to the nearly equivalent results, in particular, if the grain boundary traces have been straightened. Less satisfactory are the estimates of the spatial grain density N_V . The ASTM estimate based on the intercept count was by 40% higher than that one based on the profile count (this difference was only 10% after straightening the boundary traces). However, a more realistic estimate taking into account also the small profile area dispersion was by 30%

lower than the estimate based on the ASTM recommended formula. Such an overestimation can be expected for all grain structures with mild grain size dispersion.

- 3) The numbers of measured features for such an improved analysis was moderate (≈ 400 chords and ≈ 120 profiles) and the subsequent statistical treatment based on the w - s diagram is quite simple. However, it should be underlined that the amount of required effort quickly increases with decreasing regularity of the examined structure.

ACKNOWLEDGEMENTS

This research was supported by the Slovak Agency for Science VEGA (contract No. 2/6097/99 -- O. V., M. B.) and by the Grant Agency of the Czech Republic (contract No. 201/99/0269 -- I.S.).

REFERENCES

- [1] ČSN 42 0462: Stanovení velikosti zrna ocelí a neželezných kovů [Standards for determination of grain size in steels and non-ferrous metals -in Czech], (1982).
- [2] ASTM E-112: Standard Methods for Determining Average Grain Size (1982, 1988).
- [3] Saxl, I., Ponížil, P.: Grain size estimation: w - s diagram. *Materials Characterization* 42, 2001, 1-6.
- [4] Besterci, M., Šlesár, M., Jangg, G.: Optimalizácia parametrov mechanického legovania a kompaktizácie. *Pokroky práškové metalurgie*, 1-2, 1992, 19-31.
- [5] Besterci, M.: Disperzne spevnený hliník pripravený mechanickým legovaním. *Pokroky práškové metalurgie*, 34, 2, 1996, 5-73.
- [6] Horálek, V.: [12] V.: ASTM grain size model and related random tessellation models. *Materials Characterization*. 25 (1990) 263-284.
- [1] Saxl, I., Ponížil, P.: Grain size estimation I, II. In: L. Wojnar, K. Roźniatowski (eds.): STERMAT'2000, Proc. Sixth Int. Conf. „Stereology and Image Analysis in Materials Science, Cracow 20. - 23. 9. 2000. Cracow: Polish Society for Stereology, 2000: 373-378, 379-384.
- [8] Saxl, I., Sülleiová, K., Ponížil, P.: Simulating grain size estimation. *Kovové materiály* (in press).